PAPER

An easily modified method using FeCl₃ to synthesize nanoporous gold with a high surface area†

Kenan Shao,[a] Chun Fang,[a] Yinfang Yao,[a] Canyun Zhao,[a] Zhi Yang,[a] Jianguo Liu [ID] *[ab] and Zhigang Zou*[ab]

Here, we report a two-step dealloying method using ferric chloride to synthesize nanoporous gold (NPG), instead of the traditional corrosive nitric acid method. In the new method, the pore size can be easily controlled by using various solutions and additives. For example, when using ethylene glycol (EG) as a solvent, the NPG (NPG-EG) pore size can be made as small as 8 nm, thus increasing the electrochemical specific surface area of the NPG to seven times higher than that of traditional NPG with a pore size of 25 nm. NPG-EG showed an enhanced capacitance of 1340 F g^{-1} at a current density of 2.0 A g^{-1} when electrodeposited with Ni₃S₂.

1. Introduction

In recent years, strategies for synthesizing nanoporous materials and applications of these materials have been intensively pursued because of the strong porosity-induced enhancement of their properties.[1-6] After Jonah Erlebacher and co-workers developed the concentrated nitric acid (HNO₃) dealloying method to fabricate a nanoporous gold (NPG) leaf,[7] many results related to the usage of this material have been reported. Ling Zhang and his co-workers took advantage of wrinkled NPG films that contained abundant Raman-active nanogaps to yield surface-enhanced Raman scattering intensity.[8] Roswitha Zeis *et al.* applied platinum-plated nanoporous gold into hydrogen/oxygen fuel cells and gained a maximum power generation of ~250 mW cm^{-2} at Pt loads of ~0.03 mg cm^{-2}.[9] F. Meng and Y. Ding showed that a nano-composite of polypyrrole (PPy)-decorated NPG could form an all-solid-state supercapacitor with great volumetric capacitance and high power and energy densities.[10] However, rearrangement during dealloying is usually very rapid when involving the strong acid that is used or during alkali corrosion,[11] leaving little ability to adjust the porosity features in such nanoporous products.

In this work, we designed an easily modified two-step method using FeCl₃ to fabricate NPG and further improved the specific surface area (SSA) of the NPG by tuning the reaction

conditions. To activate the reaction, we introduced halogen ions (Cl$^-$, Br$^-$, I$^-$) to lower the oxidation potential ($E^0_{Ag^+/Ag} = +0.799$ V, $E^0_{AgCl/Ag} = +0.222$ V, $E^0_{AgBr/Ag} = +0.071$ V, $E^0_{AgI/Ag} = -0.152$ V *vs.* standard hydrogen electrode, SHE). In the presence of halogen ions, ferric ions (Fe^{3+}) and even copper ions (Cu^{2+}) were able to oxidize Ag ($E^0_{Fe^{3+}/Fe^{2+}} = +0.771$ V, $E^0_{Cu^{2+}/Cu} = +0.34$ V *vs.* SHE).

2. Experimental section

2.1 Material preparation

Films made of an alloy of Ag and 12 carat Au (Sepp Leaf Products, New York) were used to prepare nanoporous gold (NPG) films. Nitric acid (69.0%), ferric chloride (FeCl₃·6H₂O, 99.0%), ferric bromide (FeBr₃, 95.0%), copper chloride (CuCl₂, 99.0%), stannic chloride (SnCl₄, 99.0%), Na₂S₂O₃·5H₂O (99.0%) and nickel chloride (NiCl₂, 99.5%) were all purchased from Sigma-Aldrich. Other reagents employed in this work were analytically pure and used without further purification. An Au/Ag alloy film with dimensions of 2 cm by 2 cm and with an Au-to-Ag atomic ratio of 35 : 65 was floated on the surface of an FeCl₃ solution for a specified period of time. The alloy film was rinsed three times in ultra-pure water (18.2 MΩ cm), and then transferred onto a 1.0 M Na₂S₂O₃ solution to remove AgCl. At last, it was rinsed twice again. We also employed FeBr₃, CuCl₂, and SnCl₄, respectively, to prepare other NPGs in exactly the same way as we employed FeCl₃ in order to find the best oxidant.

2.2 Microstructure characterizations

The microstructure and chemical composition of the as-synthesized NPG were examined by scanning electron microscopy (SEM, NOVA NANOSEM 230, FEI, USA) equipped with

[a]Jiangsu Key Laboratory for Nano Technology, National Laboratory of Solid State Microstructures, College of Engineering and Applied Sciences, Collaborative Innovation Center of Advanced Microstructures, Nanjing University, 22 Hankou Road, Nanjing 210093, China. E-mail: jianguoliu@nju.edu.cn; zgzou@nju.edu.cn

[b]Kunshan Innovation Institute of Nanjing University, Kunshan Sunlaite New Energy Co., Ltd., 1699 South Zuchongzhi Road, Kunshan, Suzhou, 215347, China

energy dispersive spectroscopy (EDS) at 15 keV and transmission electron microscopy (TEM, TC20, FEI, USA) with EDS at 200 keV. X-ray diffraction (XRD) patterns were obtained on a Rigaku D/MAX-Ultima III X-ray diffractometer using Cu Kα radiation ($\lambda = 0.15406$ nm) with a 2θ angular range of 10° to 80° at a scan rate of 10° min^{-1}.

2.3 Electrodeposition of Ni_3S_2 and electrochemical measurements

Electrochemical measurements were taken at an electrochemical station (PARSTAT 2273, Princeton Applied Research).
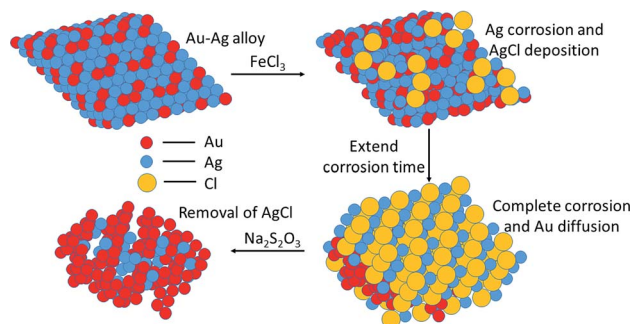
Scheme 1   Illustration of the dealloying of nanoporous gold using $FeCl_3$.

A platinum electrode and a silver chloride (Ag/AgCl) electrode served as a counter electrode and reference electrode, respectively. A glassy carbon disk with a diameter of 3 mm was employed as a working electrode. The electrochemical deposition of Ni_3S_2 using cyclic voltammetry (CV) was performed for the potential range -1.2 V to 0.2 V vs. Ag/AgCl at a scan rate of 5 mV s^{-1} for ten cycles. The deposition bath was composed of 50 mM $NiCl_2 \cdot 6H_2O$ and 1 M thiourea. An as-prepared NPG@Ni_3S_2 electrode was rinsed with deionized water and subsequently dried in vacuum conditions at 60 °C for 12 h. The mass of the electrodeposited Ni_3S_2 was measured by using an inductively coupled plasma (ICP) emission spectrometer. Cyclic voltammetry and galvanostatic charge–discharge tests were carried out using a 2.0 M aqueous KOH solution saturated with highly purified nitrogen at potentials between 0 V and 0.60 V and between -0.05 V and 0.45 V vs. Ag/AgCl, respectively.

3. Results and discussion

The morphologies of NPG films corroded using various oxidants are shown in Fig. S1.† NPG corroded using an $FeCl_3$ solution was observed to have a typical bicontinuous structure with pores similar to NPG made using HNO_3. However, $FeBr_3$ and $CuCl_2$ did not corrode the alloy completely and the pores
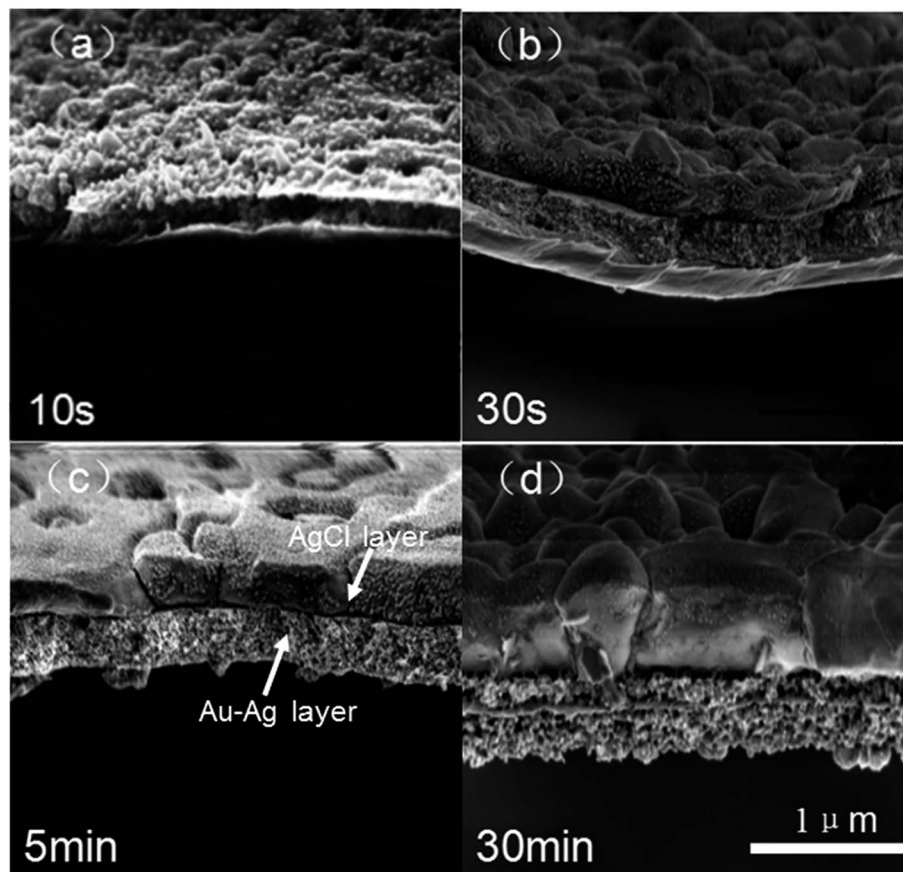

Fig. 1   (a)–(d) SEM images of a cross-section of a 400 nm-thick Au–Ag alloy at different etching times in 2 M $FeCl_3$. The AgCl layer and Au–Ag layer are labeled in (c).
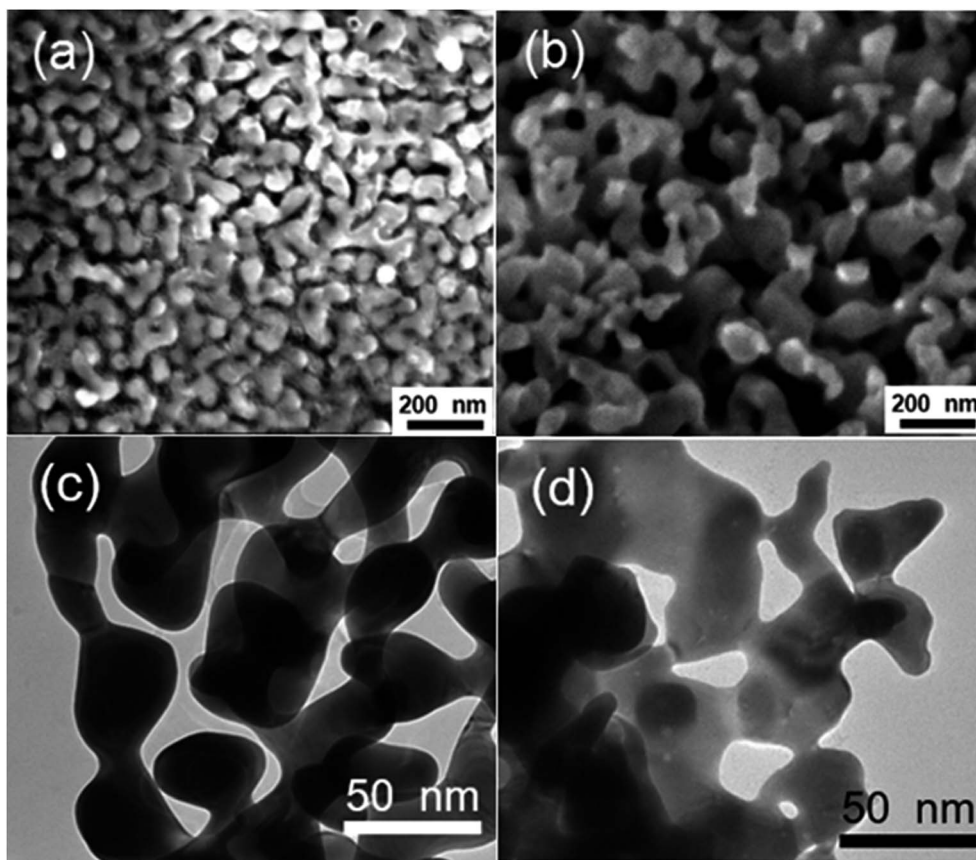
Fig. 2 (a and b) SEM and (c and d) TEM images of (a and c) NPG-N and (b and d) NPG-H.

were not distributed uniformly. Hence, the subsequent experiments were optimized using ferric chloride (denoted as NPG-H), as discussed below.

The whole dealloying process is illustrated in Scheme 1. During the reaction in the $FeCl_3$ solution, the Au–Ag alloy served as a template to guide the AgCl to nucleate.[11] The cross-section (Fig. 1) and plane-section (Fig. S2†) SEM images of the Au–Ag alloy samples at different etching times showed that the reaction took place very rapidly (in less than 30 seconds). Here, the AgCl nanocrystals grew on the surface of the alloy film by following a Volmer–Weber growth model[12] during the corrosion process and tending to the defect sites with their higher surface energy levels, while at the same time the deagglomeration of the Au atoms shaped the bicontinuous structure (denoted as NPG@AgCl). The moderate affinity between Cl^- ions and Au can help form sponge-like gold while preventing further gold diffusion.[13,14] Also, J. Snyder et al. pointed that further dissolution of Au atoms is rate-limited by dissolution of Ag from nine-coordinated terrace sites in face-centered cubic alloys.[15] So we can conclude that a higher Ag content and excess Cl^- ions can prevent further Au diffusion. Moreover, the loose morphology of AgCl cannot destroy the continuity of the reaction, so Ag atoms in the inner layer can also be fully corroded.[16] AgCl was easily removed by using a 1.0 M sodium

hyposulfite (NaS_2O_3) solution (Fig. S3†), and SEM mapping of a cross-section selected from NPG@AgCl with an etching time of 30 s (Fig. S4†) showed the relative aggregation of Au and Ag, and we concluded that Ag atoms dissolved from the alloy film and formed AgCl, and residual Au atoms formed a porous structure similar to that in NPG prepared using HNO_3.

Typical SEM and TEM images of NPG prepared using HNO_3 (denoted as NPG-N) and NPG-H are shown in Fig. 2(a)–(d). To modify the porosity of the NPG, we added polyvinyl pyrrolidone (PVP) as a surfactant in the $FeCl_3$ solution (denoted as NPG-HP) or employed EG as a solvent instead of water (denoted as NPG-EG). As shown in Fig. S5 and Table S1,† we found that the pore size of NPG decreased from about 25 nm for NPG-N and NPG-H to 10 nm for NPG-HP and 8 nm for NPG-EG. We further determined the electrochemical activity surface areas (ECSAs) of the NPG-N, NPG-H and NPG-EG electrodes, by obtaining cyclic voltammogram (CV) curves of these electrodes in 0.1 M $HClO_4$ solutions. The CV curves of all NPG samples (Fig. S6†) showed two typical Au oxidation peaks between 1.25 V and 1.55 V and a reduction peak between 1.10 V and 1.15 V. The slight negative shift of the reduction peaks relative to the oxidation peaks might have resulted from the presence of more Ag when using $FeCl_3$.[17] We calculated the ECSAs of the NPG electrodes by integrating the Au reduction peaks in the range 0.95 V to 1.40 V
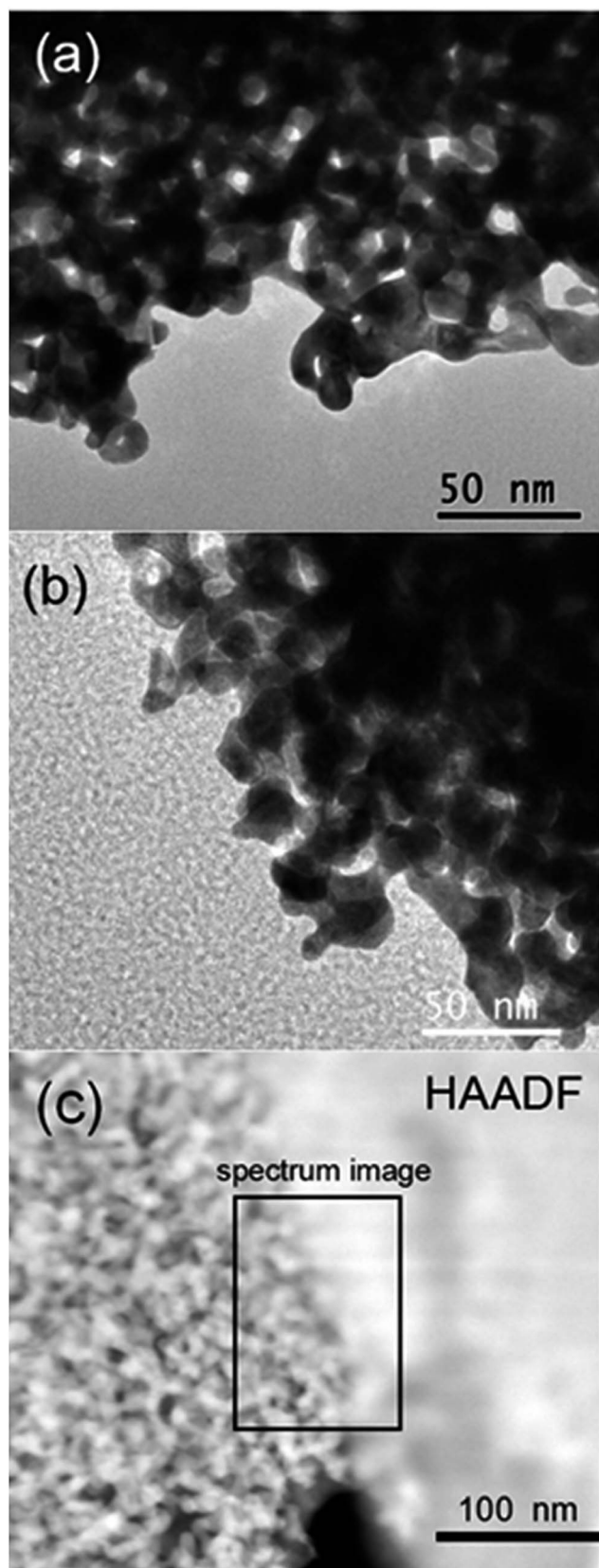
Fig. 3 (a and b) TEM images of (a) NPG–EG and (b) NPG-EG@Ni$_3$S$_2$. (c) HAADF TEM image from a selected area at the edges of the NPG-EG@Ni$_3$S$_2$ sample.

vs. RHE and then dividing the integral by a charge density of 390 μC cm^{-2}, as reported for Au.[18] The roughness factor (R_f) values (surface area/electrode area, using an electrode area of 0.196 cm^2) of NPG-N, NPG-H, NPG-HY and NPG-EG were then determined to be 8.6, 17.6, 28.3 and 62.4, respectively. Hence, NPG-EG, with a pore size one-third that of NPG-N, showed a 7.25-fold greater ECSA than did NPG-N.

In order to explore the potential of Ni$_3$S$_2$ in the electrochemical field, we electrodeposited it on NPG-EG using methods similar to those described in the paper by X. Sun and colleagues.[19] Fig. 3(a) and (b) show the TEM images of NPG-EG and NPG-EG coated with Ni$_3$S$_2$ (denoted as NPG-EG@Ni$_3$S$_2$); the porous bi-continuous structure was observed to be preserved after the electrodeposition with Ni$_3$S$_2$. The XRD spectrum of the as-grown NPG-EG@Ni$_3$S$_2$ sample (Fig. S3†) showed peaks at $2\theta = 21.7°$, 31.1°, 37.8°, 44.3° and 49.7°, which were attributed to a single crystal of Ni$_3$S$_2$ (JCPDS no. 44-1418). We chose a particular area at the edges of the NPG-EG@Ni$_3$S$_2$ sample that was not covered completely with Ni$_3$S$_2$, and observed it using a high-angle annular dark field (HAADF) TEM (Fig. 3(c)). In the HAADF image, the selected area was observed to be divided by a linear boundary, indicating an NPG/Ni$_3$S$_2$ interface. Fig. 4(a)–(c) show the Au, Ni and S elemental mappings for the area of the NPG-EG@Ni$_3$S$_2$ sample shown in Fig. 3(c). Ni and S were observed in these mappings to be distributed similarly and to be predominantly located on the right side of boundary, with Au predominantly on the left side. The mapping results and a relatively low-resolution TEM image of NPG-EG@Ni$_3$S$_2$ (Fig. S7†) showed that Ni$_3$S$_2$ was uniformly electrodeposited on the surface of the NPG and formed a double-layer structure.

Fig. 5(a) shows cyclic voltammogram (CV) curves of NPG-N@Ni$_3$S$_2$, NPG-H@Ni$_3$S$_2$ and NPG-EG@Ni$_3$S$_2$ with a scan rate of 20 mV s^{-1}. All of these curves showed explicit Ni(II) and Ni(III) redox peaks, indicating the presence of a reversible faradaic reaction and pseudocapacitive behaviour:[20]

$$Ni_3S_2 + 3OH^- \leftrightarrow Ni_3S_2(OH)_3 + 3e^- \qquad (1)$$
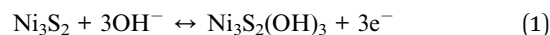
Moreover, the NPG-EG@Ni$_3$S$_2$ electrode showed a larger capacitance than did the NPG-N@Ni$_3$S$_2$ and NPG-H@Ni$_3$S$_2$ electrodes. Fig. 5(b) shows the CV curves of NPG-EG@Ni$_3$S$_2$ at different scan rates from 5.0 mV s^{-1} to 50 mV s^{-1}. The shapes of the curves remained almost unchanged, suggestive of ideal capacitive behaviours and excellent rate capabilities.[21] Fig. 5(c) shows the galvanostatic charge–discharge curves of the NPG-N@Ni$_3$S$_2$, NPG-H@Ni$_3$S$_2$ and NPG-EG@Ni$_3$S$_2$ electrodes at a current density of 2.0 A g^{-1}, and the specific capacitance values of these electrodes were found to be 224 F g^{-1}, 532 F g^{-1} and 1340 F g^{-1}, respectively. Fig. 5(d) shows the galvanostatic charge–discharge curves of the NPG-EG@Ni$_3$S$_2$ electrode at current densities from 2.0 A g^{-1} to 50 A g^{-1}, and the specific capacitance at 50 A g^{-1} was 803 F g^{-1}, i.e., nearly 60% of the capacitance was maintained.
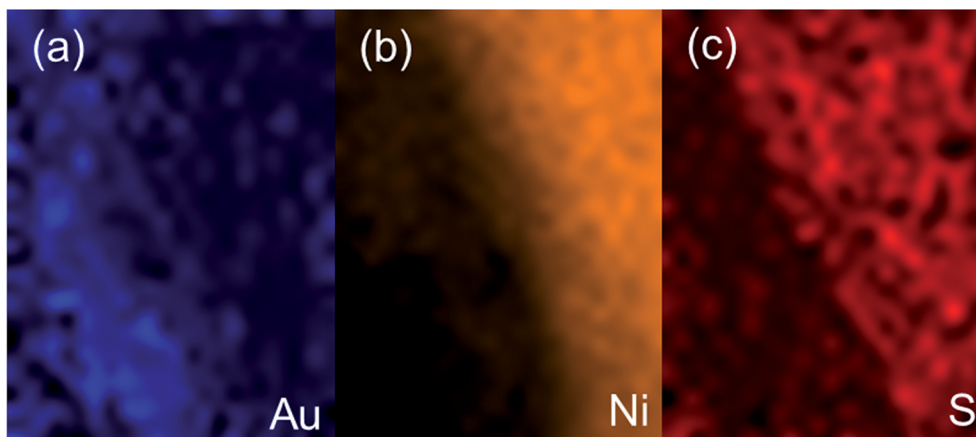
Fig. 4   HAADF TEM mapping results (from the rectangled area of Fig. 3(c)) for (a) Au, (b) Ni and (c) S.
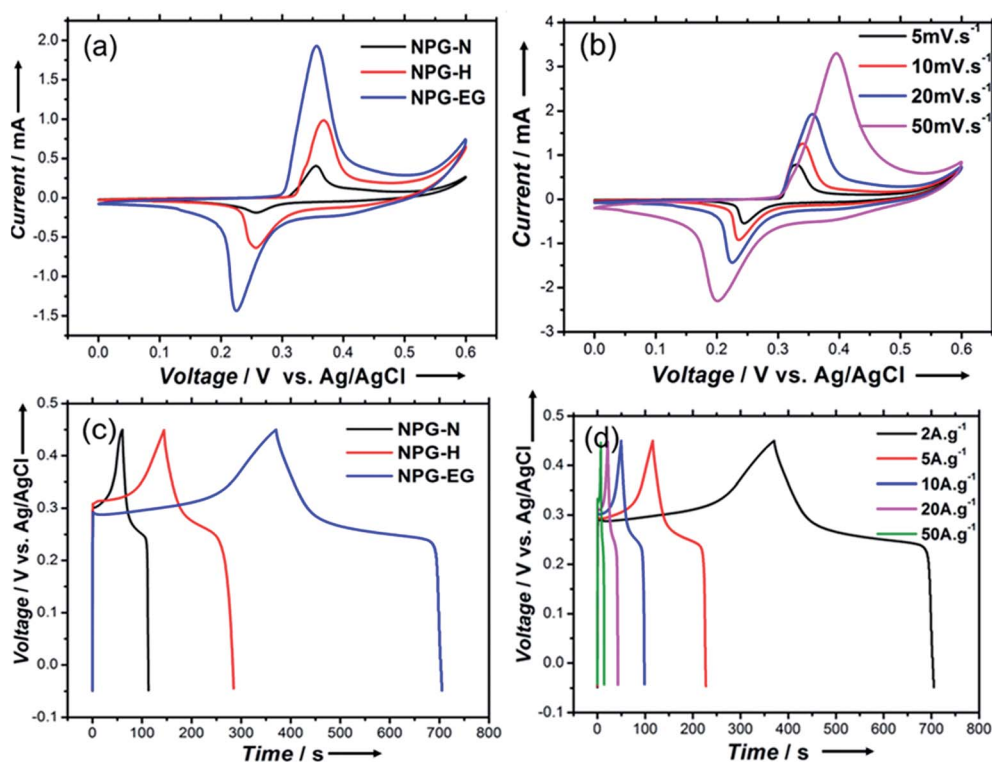

Fig. 5   (a and b) Cyclic voltammograms, in the potential range 0 V to 0.6 V, of (a) the NPG-N@Ni$_3$S$_2$, NPG-H@Ni$_3$S$_2$ and NPG-EG@Ni$_3$S$_2$ electrodes at a scan rate of 20 mV s^{-1} and (b) the NPG-EG@Ni$_3$S$_2$ electrode at various scan rates, with each of the electrodes in 2.0 M KOH. (c and d) Galvanostatic charge–discharge curves, in the potential range −0.05 V to 0.45 V, of (c) the NPG-N@Ni$_3$S$_2$, NPG-H@Ni$_3$S$_2$ and NPG-EG@Ni$_3$S$_2$ electrodes at a current density of 2.0 A g^{-1} and (d) the NPG-EG@Ni$_3$S$_2$ electrode at various current densities, with each of the electrodes in 2.0 M KOH.

4.   Conclusions

In summary, we have successfully synthesized nanoporous gold by using an FeCl$_3$ solution. Due to the AgCl growing as "islands", the NPG@AgCl template fabricated using FeCl$_3$ apparently prevented further diffusion of Au atoms and made the porosity of the products controllable when just using a surfactant like PVP or replacing the corrosion reaction solvent with EG. Including the

EG solvent reduced the pore size of the NPG from 25 nm to about 8 nm. Introducing EG, by apparently causing the ions to move more slowly, reduced the rate of dealloying, hence creating a more delicate structure and more catalytic sites, and leading to a better catalytic performance. Consequently, compared to NPG made using previous methods, the NPG made using our new methods performed better as a substrate of a supercapacitor coated with Ni$_3$S$_2$. In conclusion, our methods offer increased

possibilities for using porous metals in a variety of fields such as photocatalysis or Li–S batteries.

Notes and references

1 R. Ryoo, S. H. Joo, M. Kruk and M. Jaroniec, *Adv. Mater.*, 2001, **13**, 677–681.
2 H. Furukawa, N. Ko, Y. B. Go, N. Aratani, S. B. Choi, E. Choi, A. O. Yazaydin, R. Q. Snurr, M. O'Keeffe, J. Kim and O. M. Yaghi, *Science*, 2010, **329**, 424–428.
3 R. K. Dash, G. Yushin and Y. Gogotsi, *Microporous Mesoporous Mater.*, 2005, **86**, 50–57.
4 A. H. Lu and F. Schuth, *Adv. Mater.*, 2006, **18**, 1793–1805.
5 T. Nakamura, Y. Yamada and K. Yano, *J. Mater. Chem.*, 2007, **17**, 3726–3732.
6 Y. Lei, J. Lu, X. Y. Luo, T. P. Wu, P. Du, X. Y. Zhang, Y. Ren, J. G. Wen, D. J. Miller, J. T. Miller, Y. K. Sun, J. W. Elam and K. Amine, *Nano Lett.*, 2013, **13**, 4182–4189.
7 J. Erlebacher, M. J. Aziz, A. Karma, N. Dimitrov and K. Sieradzki, *Nature*, 2001, **410**, 450–453.
8 L. Zhang, X. Y. Lang, A. Hirata and M. W. Chen, *ACS Nano*, 2011, **5**, 4407–4413.
9 R. Zeis, A. Mathur, G. Fritz, J. Lee and J. Erlebacher, *J. Power Sources*, 2007, **165**, 65–72.
10 F. Meng and Y. Ding, *Adv. Mater.*, 2011, **23**, 4098–4102.
11 Y. G. Sun, *J. Phys. Chem. C*, 2010, **114**, 2127–2133.
12 V. L. K. Oura and A. Saranin, *et al.*, *Surface Science: An Introduction*, Springer, 2010.
13 A. Dursun, D. V. Pugh and S. G. Corcoran, *J. Electrochem. Soc.*, 2003, **150**, B355–B360.
14 Z. Zhang, H. Li, F. Zhang, Y. Wu, Z. Guo, L. Zhou and J. Li, *Langmuir*, 2014, **30**, 2648–2659.
15 J. Snyder and J. Erlebacher, *J. Electrochem. Soc.*, 2010, **157**, C125–C130.
16 Y. Bi and J. Ye, *Chem. Commun.*, 2009, 6551–6553.
17 M. Tominaga, T. Shimazoe, M. Nagashima, H. Kusuda, A. Kubo, Y. Kuwahara and I. Taniguchi, *J. Electroanal. Chem.*, 2006, **590**, 37–46.
18 D. A. J. Rand and R. Woods, *J. Electroanal. Chem.*, 1972, **35**, 209–218.
19 Z. Xing, Q. Chu, X. Ren, C. Ge, A. H. Qusti, A. M. Asiri, A. O. Al-Youbi and X. Sun, *J. Power Sources*, 2014, **245**, 463–467.
20 S. W. Chou and J. Y. Lin, *J. Electrochem. Soc.*, 2013, **160**, D178–D182.
21 W. Zhou, X. Cao, Z. Zeng, W. Shi, Y. Zhu, Q. Yan, H. Liu, J. Wang and H. Zhang, *Energy Environ. Sci.*, 2013, **6**, 2216–2221.